4-2012

In-situ investigation of phase formation in nanocrystalline (Co97.5Fe2.5)89Zr7B4 alloy by high temperature x-ray diffraction

Samuel J. Kernion
Carnegie Mellon University

Paul Ohodnicki
National Energy Technology Laboratory

Michael E. McHenry
Carnegie Mellon University, mm7g@andrew.cmu.edu

Published In
Journal of Applied Physics, 111, 7, 07A316.

In-situ investigation of phase formation in nanocrystalline $(Co_{97.5}Fe_{2.5})_{89}Zr_7B_4$ alloy by high temperature x-ray diffraction

Samuel J. Kernion,[1,a)] Paul R. Ohodnicki,[2] and Michael E. McHenry[1]
[1]*Materials Science and Engineering Department, Carnegie Mellon University, Pittsburgh, Pennsylvania 15213, USA*
[2]*National Energy Technology Laboratory, Chemistry and Surface Science Division, Pittsburgh, Pennsylvania 15236, USA*

(Presented 1 November 2011; received 23 September 2011; accepted 29 October 2011; published online 16 February 2012)

Crystallization and phase evolution in an $(Co_{97.5}Fe_{2.5})_{89}Zr_7B_4$ amorphous alloy was studied by high temperature x-ray diffraction (HTXRD) and transmission electron microscopy (TEM). Co-based nanocomposite alloys have zero magnetostriction and a strong response to magnetic field annealing making them interesting for sensor and high frequency power applications. Amorphous alloys, synthesized by single roll melt-spinning, develop a nanocomposite structure after primary crystallization. After annealing at 540 °C for 1 h, TEM images and diffraction patterns confirm a grain size of 19 nm and the presence of at least two phases. HTXRD results show preferential body centered cubic (bcc) nucleation and formation of multiple phases at various stages of crystallization. Only the face centered cubic (fcc) phase remained at temperatures above 600 °C. On heating, the lattice parameter of the fcc phase increases at a rate higher than expected from thermal expansion. This is partially explained by an increase in the Fe-concentration in fcc crystallites. © *2012 American Institute of Physics*. [doi:10.1063/1.3673433]

I. INTRODUCTION

Nanocomposite magnets are of considerable interest due to soft magnetic properties, high magnetic flux densities[1] and high frequency response with low losses as compared to bulk metals such as Si-steels.[2] Fe-based alloys have attracted the most attention, as optimized alloys exhibit relatively high magnetic flux densities and low losses. Co-based alloys, with small or zero magnetostriction, a relatively large response to magnetic field annealing[3–8] and excellent mechanical properties making them interesting for magnetic sensors and high frequency applications.[9,10]

In transforming amorphous precursors to nanocomposite magnets, it is possible to suppress stable phase formation and exploit properties of metastable phases. Recent suppression of the nucleation of the γ-phase has been observed in Co-Fe-based nanocomposites at compositions where the binary Fe-Co phase diagram predict that the α- and $\tilde{\gamma}$phases coexist.[3–8] In Fe-Ni-based nanocomposites, similar observations in Fe-rich alloys[11] show nucleation of the γ-phase is suppressed in favor of a metastable α-phase.

$(Co_{100-x}Fe_x)_{89}Zr_7B_4$ ($x = 0-5$) alloys are remarkable in that three phases [body centered cubic (bcc), face centered cubic (fcc), and hexagonal close packed (hcp)] can form simultaneously during the annealing process, even though the bulk Fe-Co binary phase diagram suggests that only fcc would form at typical isothermal crystallization temperatures. In the context of classical nucleation theory, previous work postulated that preferential nucleation of bcc crystallites in Co-rich alloys could be potentially explained in terms of strain and/or interfacial energy effects.[5–7] The possibility of hcp phase formation arises from similar free energies of the hcp and fcc phases and, in some cases, it is difficult to unambiguously identify grains as hcp or fcc because of a high density of stacking faults.

Here, *in-situ* high temperature x-ray diffraction (HTXRD) studies are used to further explore the crystallization of amorphous $(Co_{97.5}Fe_{2.5})_{89}Zr_7B_4$ alloy. HTXRD enables rapid characterization of the phase evolution throughout the crystallization process as well as the temperature dependence of the lattice parameter. With such information, annealing treatments can be tailored to achieve desired phases and resulting properties and the chemical partitioning between various phases during crystallization can be studied.

II. EXPERIMENTAL PROCEDURES

A 50 g ingot, with nominal composition $(Co_{97.5}Fe_{2.5})_{89}Zr_7B_4$, was synthesized by arc melting elemental constituents. The remelted ingot was rapidly quenched by melt-spinning in a low pressure Ar atmosphere onto a water cooled Cu-Be wheel rotating at 50 m/s. Cast ribbon was 3 mm wide, 30 mm thick, and many meters long. A portion of the ribbon was encapsulated in an Ar atmosphere and annealed at 540 °C for 1 h. The microstructure of the annealed ribbon was examined by transmission electron microscopy on a JEOL 2000EX with a 200 kV beam voltage.

For high temperature XRD, as-cast ribbon was cut and placed so that a 1 cm diameter quartz wafer was covered by the ribbon. Boron nitride (BN) spray was used to affix the ribbons to the wafer. Scans were taken on a Panalytical X'Pert Pro diffractometer with a Cu radiation source ($\lambda = 0.154$ nm). Each scan had an effective scan time of 12 ks over the 2θ range of 35–55° with the use of a line detector. An Anton Paar HTK-1200 Oven was used to heat the sample under nitrogen. Patterns were recorded from 50 to 700 °C, during heating and cooling with a 10 °C/min rate between scans. Alumina

a)Electronic mail: skernion@andrew.cmu.edu.

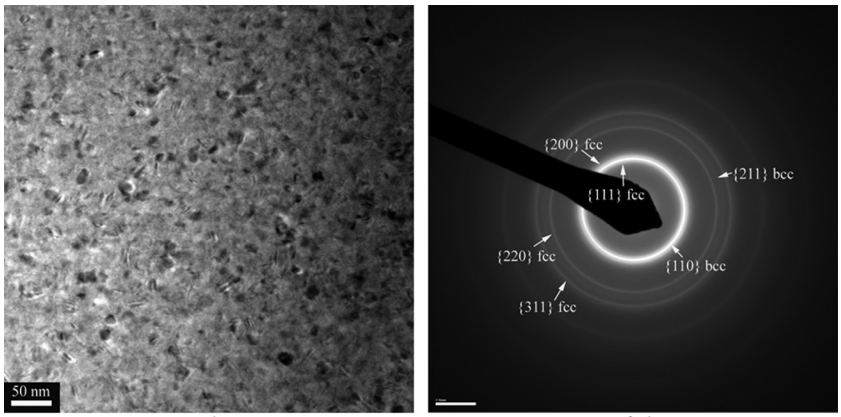

FIG. 1. (a) Bright field TEM image of $(Co_{97.5}Fe_{2.5})_{89}Zr_7B_4$ after annealing at 540 °C for 1 h displaying the size of the nanograins and (b) the corresponding diffraction ring pattern.

powder was used as a reference material. Peaks were fit by a Cauchy-Lorentz distribution using Igor Pro©TM software.

III. RESULTS AND DISCUSSION

The TEM bright field image of Fig. 1 taken after annealing displays a nanocrystalline microstructure with grain size of 19.2 +/−3.9 nm. The diffraction pattern shows a broad first ring, corresponding to the {110} bcc ring and bordering {111} and {200} fcc rings. Rings corresponding to other fcc and bcc planes confirm their presence. There is no evidence of the hcp phase, however, a peak from the hcp phase may be unresolved in the first ring.

Figure 2 displays the results of XRD experiments. The as-cast sample displays a broad, low intensity peak centered at 44° typical of Co and Fe based amorphous materials. The first indication of crystallization appears in an increase in intensity and narrowing of the amorphous peak at 400 °C. As the peak is centered at 45.0°, it is attributed to {110} bcc planes consistent with the prior results.[4,12] At 500 °C, the {111} fcc peak emerges centered at 44.1°. As temperature is increased, the {110} bcc peak eventually recedes while the {111} fcc peak continues to grow. This is consistent with observations in prior work for this alloy system.[3–8] At 600 °C a broad peak at 47.0° suggests crystallites with hcp stacking rather than fcc. As temperature is further increased this peak disappears at the expense of continued growth of the corresponding fcc peaks up to 700 °C. Peaks due to a secondary crystalline phase, typically $(Co,Fe)_{23}Zr_6$ or $(Co,Fe)_2Zr$,[3] do not appear in the high temperature XRD patterns obtained here. Further work would be required to clarify the lack of such peaks with potential causes including (1) low resolution of scans due to a need to balance kinetic factors with signal to noise ratio and (2) a potential depletion of glass formers at the ribbon surface noted in prior work on higher Fe-containing alloys.[13]

The main peaks of each phase were compared to obtain their volume fractions in order to quantitatively elaborate on the above discussion. The volume fraction (f_i) of a phase was found by taking the ratio of the integrated intensity of its main peak (e.g. {111} fcc peak) over the summed integrated intensities of the main peaks of all four phases. Volume fraction of each phase as a function of temperature is shown in Fig. 3. It is worth noting that at 600 °C there is a strong presence of all three crystalline phases. While no secondary crystallization peaks were observed, the disappearance of the amorphous peak is a good indication that the residual amorphous matrix has crystallized, likely into a secondary phase such as $(Co,Fe)_{23}Zr_6$ or $(Co,Fe)_2Zr$.

The fcc lattice parameter, calculated from the {111} peak using Bragg's law, is plotted as a function of temperature in Fig. 4. The lattice parameter shows a sharp increase on heating and on cooling follows a linear decline. The difference in the lattice parameter on heating and cooling is attributed to compositional changes and lattice strain. As shown above, after 500 °C the bcc phase begins to diminish

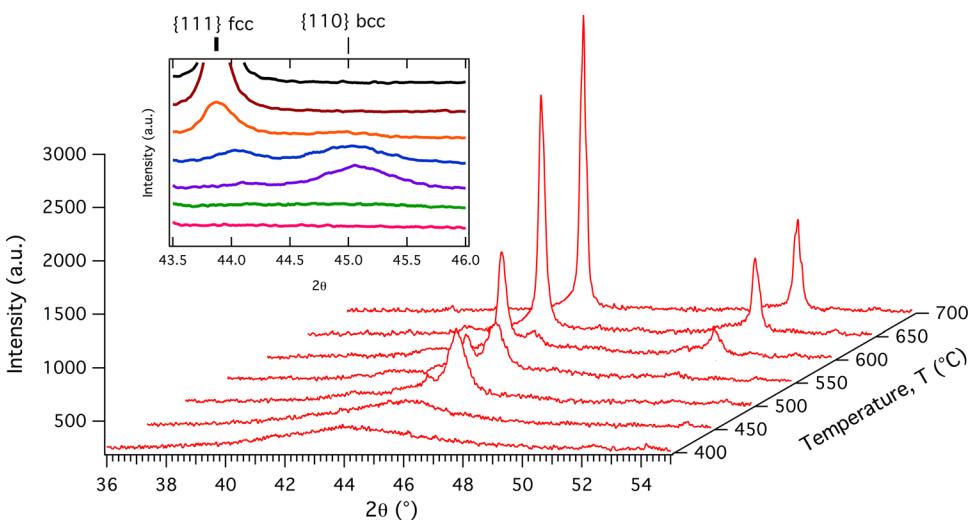

FIG. 2. (Color online) XRD diffraction patterns of $(Co_{97.5}Fe_{2.5})_{89}Zr_7B_4$ taken at temperatures between 30 and 700 °C during heating. The inset shows a close up of the {111} fcc and {110} bcc peaks.

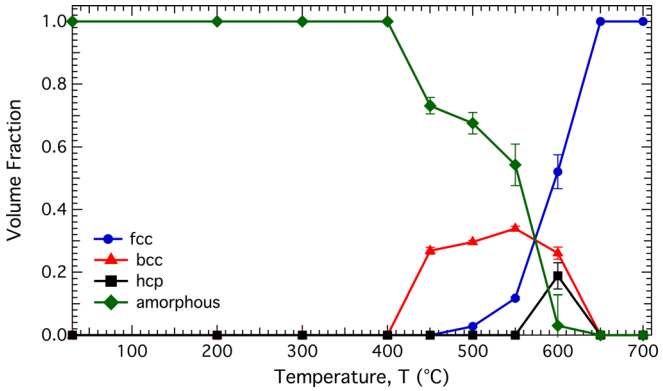

FIG. 3. (Color online) Phase volume fraction vs. temperature.

and the fcc phase grows. The bcc phase is relatively Fe-rich,[4] and as it transforms, the growing fcc phase should have a higher Fe content than grains formed at lower temperatures. This causes an increase in the lattice parameter. The bcc lattice parameter was calculated from the {110} peak and also displayed an increase that is inconsistent with thermal expansion, although the increase was half as large as the fcc lattice parameter shift in terms of their respective lattice parameters.

To estimate the Fe-content of the fcc grains as a function of temperature, the following assumptions were made: (1) initial fcc grains are entirely Co, (2) strain at the interface with a bcc grain or amorphous matrix was ignored, (3) Zr and B inside the fcc grain is not explicitly accounted for, and (4) the calculated thermal expansion could be used regardless of Fe-concentration in the fcc crystallite. The effect of the at. % of Fe (x_{Fe}) on the lattice parameter at room temperature (a_0) was predicted by

$$a_0 = \Delta a_{Fe} \bullet x_{Fe} + a_{Co}. \quad (1)$$

where Δa_{Fe} is the change in lattice parameter per at.% of Fe and a_{Co} is the lattice parameter assuming only Co comprises the fcc grain. Value of Δa_{Fe} for the bulk (Fe,Co) alloy is 0.00011 nm/at. % Fe (Ref. 14) and 0.00055 nm/at. % Fe for the $(Co_{100-x}Fe_x)Zr_7B_4$ nanocrystalline material from Ohodnicki.[4,8] The temperature dependence of lattice parameter was assumed to follow the thermal expansion expression:

$$a_{fce} = a_0(1 + \alpha T). \quad (2)$$

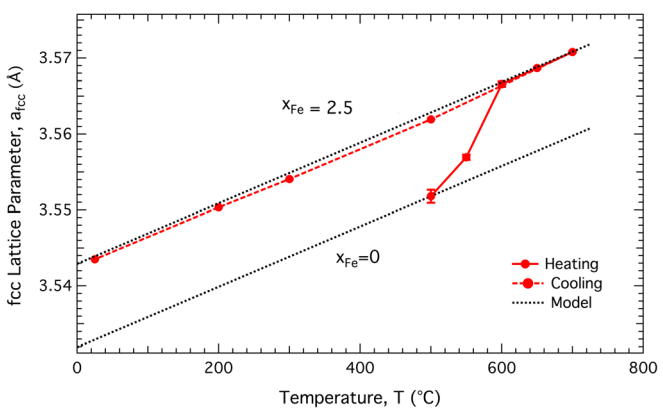

FIG. 4. (Color online) Lattice parameter of the fcc phase as a function of temperature. The dotted lines show the predicted lattice parameter.

The thermal expansion coefficient of fcc grains (a) determined from data acquired on cooling was calculated to be 1.13×10^{-5} 1/K. The lower dotted lines in Fig. 4 represents Eq. (2) with $x_{Fe} = 0$ and the dotted line that aligns closely with the data on cooling corresponds to $x_{Fe} = 9.5$ and 2.5 when the bulk and nanocrystalline values of Δa_{Fe} are used. Using the bulk value of Δa_{Fe} and performing a mass balance the maximum fcc phase fraction would be 0.26. Conversely, with the nanocrystalline value of Δa_{Fe}, the maximum fcc phase fraction would be 1, which agrees with the HTXRD results. This suggests that Fe substitution is only partially responsible for the lattice expansion. Previous results show that Zr and B solubility in the fcc grain may increase slightly with Fe content.[4] Incorporation of Zr and B into the fcc grain either by substitution or interstices may impact the lattice parameter. With an atomic radius larger than that of Co and Fe, Zr substitution for either would strain the lattice. Interactions between B or Nb with Fe are no more favorable than those with Co.[15] Further work is required to clarify the trend of increasing glass former concentration in the fcc phase with increasing Fe content.

IV. CONCLUSIONS

Phase formation in the devitrification of $(Co_{97.5}Fe_{2.5})_{89}Zr_7B_4$ amorphous alloy was studied by TEM and HTXRD. In both experiments multiple phases were found. The mechanism of phase formation in this complex alloy is still not entirely known, although these findings support previous notions of preferential bcc nucleation followed by nucleation and growth of the fcc phase. A larger than expected increase in the lattice parameter on heating of the fcc crystallites is likely indicative of changing composition in the fcc phase. The overall shift cannot be explained based upon reasonable assumptions about the change in Fe:Co ratio alone. Additional contributions may include increasing solubility of glass formers in the fcc grain with increasing Fe content.

[1]M. E. McHenry, M. A. Willard, and D. E. Laughlin, Prog. Mater. Sci. **44**, 291 (1999).
[2]S. J. Kernion, K. J. Miller, S. Shen, V. Keylin, J. Huthand, and M. E. McHenry, IEEE Trans. Magn. **47**, 3452 (2011).
[3]P. R. Ohodnicki, Jr., S.Y. Park, H. K. McWilliams, K. Ramos, D. E. Laughlin, and M. E. McHenry, J. Appl. Phys. **101**, 09N108 (2007).
[4]P. R. Ohodnicki, Y. L. Qin, D. E. Laughlin, M. E. McHenry, M. Kodzuka, and T. Ohkubo, Acta Mater. **57**, 87 (2009).
[5]P. R. Ohodnicki, P. R. Y. L. Qin, D. E. Laughlin, M. E. McHenry, and V. Keylin, J. Magn. Magn. Mater. **322**, 315 (2010).
[6]P. R. Ohodnicki, Jr., J. Long, D. E. Laughlin, M. E. McHenry, and V. Keylin, J. Appl. Phys. **104**, 113909 (2008).
[7]P. R. Ohodnicki, Jr., D. E. Laughlin, M. E. McHenry, and M. Widom, Acta Mater. **58**, 4804 (2010).
[8]P. R. Ohodnicki, Jr., Thesis, Materials Science and Engineering Department, Carnegie Mellon University (2008).
[9]A. Chaturvedi, N. Laurita, A. Leary, M. H. Phan, M. E. McHenry, and H. Srikanth, J. Appl. Phys. **109**, 107C706 (2011).
[10]N. Laurita, A. Chaturvedi, A. Leary, C. Bauer, C. Miller, M. H. Phan, M. E. McHenry, and H. Srikanth, J. Appl. Phys. **109**, 07B508 (2011).
[11]A. L. Greer and I. T. Whitaker, Mater. Sci. Forum **386-388**, 77 (2002).
[12]M. A. Willard, T. M. Heil, and R. Goswami, Metall, Mater, Trans. A **38**, 725 (2007).
[13]F. Johnson, Thesis, Materials Science and Engineering Department, Carnegie Mellon University (2003).
[14]W. C. Ellis and E. S. Greiner, Trans. ASME **29**, 415 (1941).
[15]A. Takeuchi and A. Inoue, Mater. Trans., JIM **41**, 1372 (2000).